Radiation induced luminescence of the CdZnTe substrate in HgCdTe detectors for WFC3

Augustyn Waczynski[*a], Paul W. Marshall[b], Cheryl J. Marshall[c], Roger Foltz[d],
Randy A. Kimble[c], Scott D. Johnson[a], Robert J. Hill[e]
[a]GST, NASA Goddard Space Flight Center, Greenbelt, MD 20770
[b]Consultant, Brookneal, VA 24528
[c]NASA Goddard Space Flight Center, Greenbelt, MD, 20771
[d]Sigma Space, NASA Goddard Space Flight Center, Lanham, MD, 20706
[e]SSAI, NASA Goddard Space Flight Center, Lanham, MD, 20706

ABSTRACT

Proton induced luminescence in the HgCdTe detectors for the Wide Field Camera 3 instrument has been investigated. A radiation experiment has been conducted to localize the source of the luminescence. Conclusive evidence is shown that the luminescence originates in the CdZnTe substrate and propagates toward HgCdTe photodiodes as ~800 nm radiation. Luminescence is proportional to the proton energy deposited in the substrate. Subsequent testing of detectors with the substrate removed confirmed that substrate removal completely eliminates proton induced luminescence.

Keywords: CdZnTe, HgCdTe, luminescence, focal plane arrays, radiation effects

1. INTRODUCTION

Wide Field Camera 3 (WFC3) is an instrument intended as a replacement for Wide Field Planetary Camera 2, presently on the Hubble Space Telescope (HST). WFC3 has two channels: the UVIS which covers 0.2 μm to 1.0 μm, and the IR which covers 0.8 μm to 1.7 μm. The IR channel uses a 1k x 1k HgCdTe detector, where the detector layer has been grown on a CdZnTe substrate with molecular beam epitaxy (MBE). This process which is relatively new to IR detector technology replaced the previous PACE process and resulted in significant performance improvement. The resulting reduction in detector dark current has enabled WFC3 to use thermoelectric cooling for 150K operation and to build a relatively inexpensive IR camera.

As part of the space qualification process, the detector was exposed to a radiation fluence equivalent to that of five years of service. The primary goals of the testing were to 1) verify the effect of the expected relatively benign HST dose of 0.5 krad on the dark current, similar to previous testing of the Near Infrared Camera and Multi-Object Spectrometer (NICMOS) and the Space Infrared Telescope Facility (SIRTF), and 2) to investigate the transient effects produced by doses corresponding to in-flight crossings of the South Atlantic Anomaly. Subsequent testing lead to the realization that the CdZnTe substrate is luminescent when exposed to protons representative of the primary source of dose in HST's orbit.

2. BACKGROUND

The first radiation testing of the WFC3 IR detector took place at Crocker Nuclear Laboratory (CNL) at UC Davis in November 2002. The detector was exposed to a 63 MeV proton beam while under operational conditions and a variety of images were collected [1]. Some images were collected during the radiation exposure to check for single event upsets (SEU) for transient analysis. In those images, an unexpected increase in the background signal was noted, and it appeared as a global increase in addition to the localized transient signatures of individual proton hits. Even after careful re-analysis of the experiment, an explanation for the additional background was not identified. Since CdZnTe photoluminescence has been well known [2], suspicion grew that the excessive background may have resulted from

* aw@tophat.gsfc.nasa.gov

Focal Plane Arrays for Space Telescopes II, edited by Thomas J. Grycewicz, Cheryl J. Marshall,
Proceedings of SPIE Vol. 5902 (SPIE, Bellingham, WA, 2005) · 0277-786X/05/$15 · doi: 10.1117/12.617716

radiation-induced luminescence in the substrate. When the radiation data were scaled to that of a space environment, the effect was strong enough to compromise the detector dark current performance, and the WFC3 instrument team decided to investigate further.

In May 2004, a flight-like detector (FPA67) was radiation tested at CNL. An experiment was designed to identify the source of the background seen in November 2002, and the results delivered conclusive evidence that proton energy deposited in the substrate is converted into photons, which are then detected by the detector HgCdTe diodes and are therefore responsible for an increased background.

In October 2004, WFC3 procured engineering samples of detectors with removed substrates (FPA94 and FPA95). In December 2004, these new detectors were radiation-tested to verify that substrate removal is the solution to the problem, and testing fully confirmed the expected results.

3. TEST SETUP

The WFC3 IR detector is a 1024x1024 pixel HgCdTe array hybridized to a silicon readout multiplexer. The multiplexer is a scaled down custom version of the Hawaii-2 design [3]. The detector has a format of 1024 x 1024 pixels with 5 rows and 5 columns of reference pixels on each side. The pixel size is 18 x 18 μm^2 and the detector readout is subdivided into four quadrants, each with a 512 x 512 pixel format.

The standard WFC3 readout rate of 100 kHz was maintained for all data acquisition, and all measurements were performed at 150 K. During radiation exposures, the detector was in close proximity to the proton accelerator. All post-exposure files were collected outside of the accelerator space so that spurious transients due to the increased background radiation would be minimized.

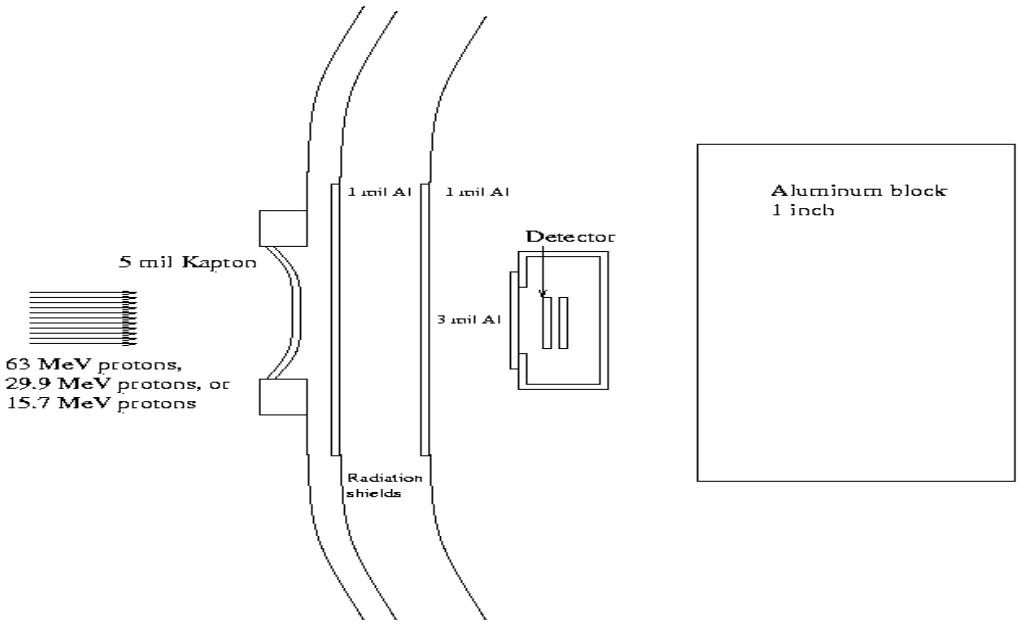

Figure 1. Detector cryostat in reference to the proton beam

The experimental setup of the IR detector in reference to the proton beam is shown in Figure 1. The detector was placed in a dewar with a 0.005 inch kapton window and three thermal shields equipped with windows, each masked by 0.001 inch thick aluminum foils, resulting in a total of 0.003 inch of aluminum between the proton beam and the detector.

The proton beam was shaped to a size of 1.5 x 1.5 inch by an aluminum aperture. The size of the dewar window exceeded 2.3 inches in diameter and the proton beam was aligned to avoid interaction with the thick vacuum shell in front of the detector. The proton beam was intentionally shaped larger than the detector in order to illuminate the detector with a uniform central section of the beam (resulting beam uniformity has been shown in Figure 8 as a line with squares).

Normal incidence was used for all tests. The proton energy was 63.3 MeV for the initial tests, and in later tests lower energies were also produced by tuning the cyclotron to vary the proton penetration depth into the CdZnTe substrate layer.

4. EXPERIMENT

FPA67, a prototype of the WFC3 flight detector with a nominal 0.8 mm thick substrate, was characterized at the Detector Characterization Laboratory (DCL) of Goddard Space Flight Center and moved to CNL at UC Davis for proton irradiation. The detector was assembled into a cryostat, brought to operational conditions, and baseline measurements were acquired. Within approximately 24 hrs of cool down, the detector was exposed to proton radiation.

The goal of the experiment was to identify the source of the additional background signal. During the test design phase, proton transport through the detector layers was modeled with the SRIM (Stopping and Ranges of Ions in Matter) simulation program [4]. A set of proton energies was established with the aim that each would penetrate the detector assembly layers to a certain depth and therefore would selectively probe different detector layers for the luminescence. The accelerator energy was set to 63.3 MeV, 29.9 MeV, and 15.7MeV, depending on the phase of the experiment. Intermediate energies were achieved by inserting aluminum sheets of varying thickness between the accelerator output window and the dewar entrance window.

Since the readout rate of WFC3 detectors is slow, the proton flux to achieve resolution of individual proton strikes had to be adjusted to levels below $10^3/cm^2/sec$ which is also well below the threshold of the existing beamline dosimetry. As a consequence, the proton flux was measured directly from the acquired images and flux stability could be lower than optimal. The objectives of the second set of experiments were to first reproduce the conditions of the previous testing when the excess background was originally noted, and then to identify the source of the background and to explore its behavior.

5. RESULTS

The first set of images, acquired with low proton hit density and the 63.3 MeV proton beam, showed a strong background signal, even stronger than that observed in the original experiment. The background was highly non-uniform across the detector area, and it was easy to notice that its shape has a strong correlation to the detector's quantum efficiency (QE) distribution at 800 nm. Figure 2 shows images of the background and the QE. Closer comparison reveals a significant difference: the ratio of peak to valley in the background approximately equals 6, while peak to valley in the QE image is no more than 2. Nevertheless, the strong correlation between QE and background indicated that the mechanism of the background generation involves short wavelength photon radiation.

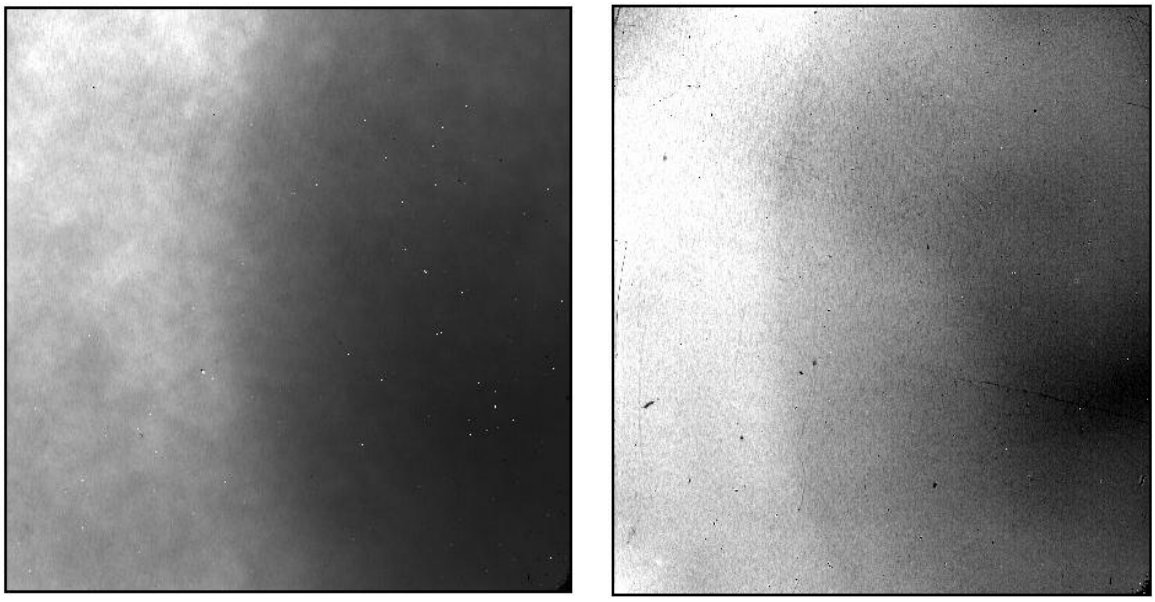

Figure 2. Comparison of the radiation background (left) with an 800 nm flat-field image (right).

To track non-uniformity of the background across the detector, one section was selected in proximity to each the four corners. Each section consisted of 100x100 pixels. The mean values for background and proton fluence are derived for each section and shown in the following figures.

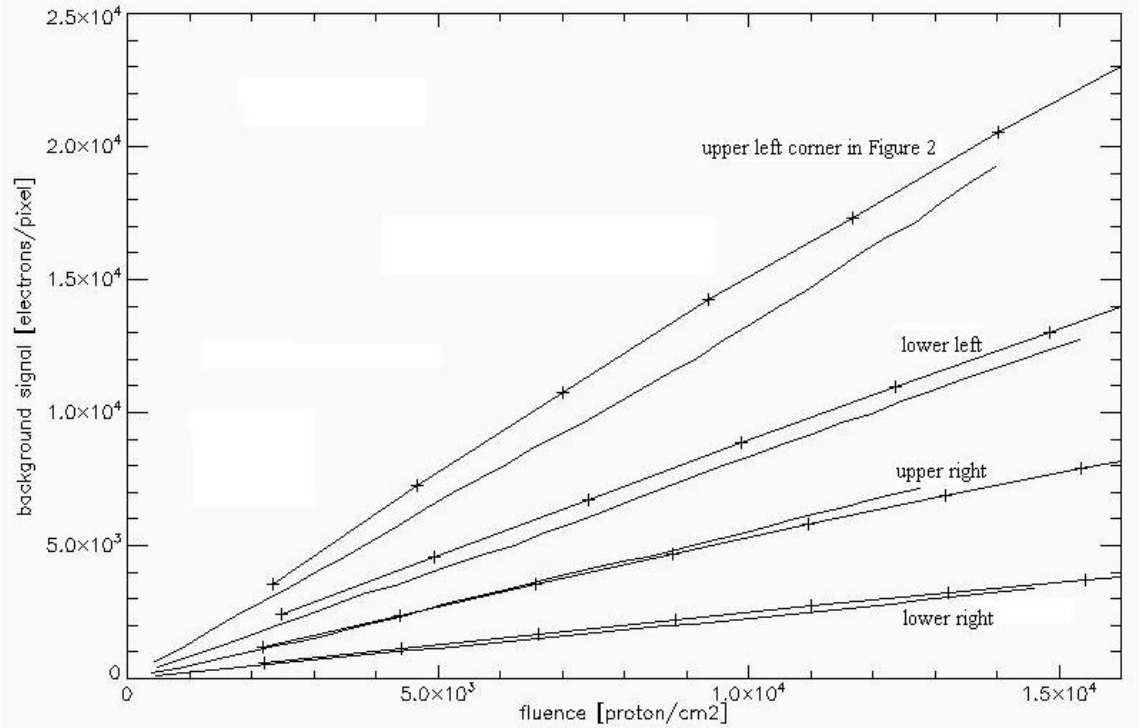

Figure 3. Four sections of 100x100 pixels placed in four corners of the image are used to compute mean background per pixel and mean fluence. The mean signal value of each section is plotted as a function of fluence for two levels of flux: the lines with marks correspond to a flux of 535 protons/sec/cm^2, while unmarked lines correspond to a flux of 100 protons/sec/cm^2. Each pair of marked and unmarked lines represents the results of one section.

The proton flux in ground-based radiation testing typically exceeds that of a space environment by many orders of magnitude. Our testing was not an exception, and attempts were made to reduce the flux level as much as possible and to capture any possible nonlinear effects. Figure 3 shows background as a function of fluence, with flux being a parameter. The difference between the marked lines representing higher flux and unmarked lines representing approximately five times lower flux may be an indication of process non-linearity, or it could be caused by an error in counting proton events due to activation of the cryostat. The existing data is not sufficient to estimate linearity with high confidence. Figure 3 also demonstrates that, to a first order approximation, background is a linear function of fluence for a given proton energy.

The background images (as in Figure 2) are highly non uniform. They show local maxima of the background in proximity to randomly distributed proton transients. An attempt was made to estimate the radius of interaction by studying the shape of the proton transient. Figures 4a and 4b show a line plot through an average single proton event. A few thousand well-isolated proton events were centered and averaged in an attempt to detect the expected increase in background in the immediate neighborhood of the proton-induced charge. Figure 4a compares proton transient line plots for detectors with the CdZnTe substrate present while Figure 4b shows the same for a detector with the substrate removed. The plots are normalized since the magnitude of the transient in the detector with substrate present was more than twice that of the detector without substrate. The size of the transient appears to be unrelated to presence or absence of the substrate: similar variation in the transient size was observed between detectors with substrate present but originating from different manufacturing runs (see Table 1).

There is a noticeable difference in the shape of proton transient between the two cases, although it was difficult to derive the range of the proton-induced background because the proton hit density was relatively high. The transient shape in Figure 4a shows an increase in peak width most prominent at the base of the event.

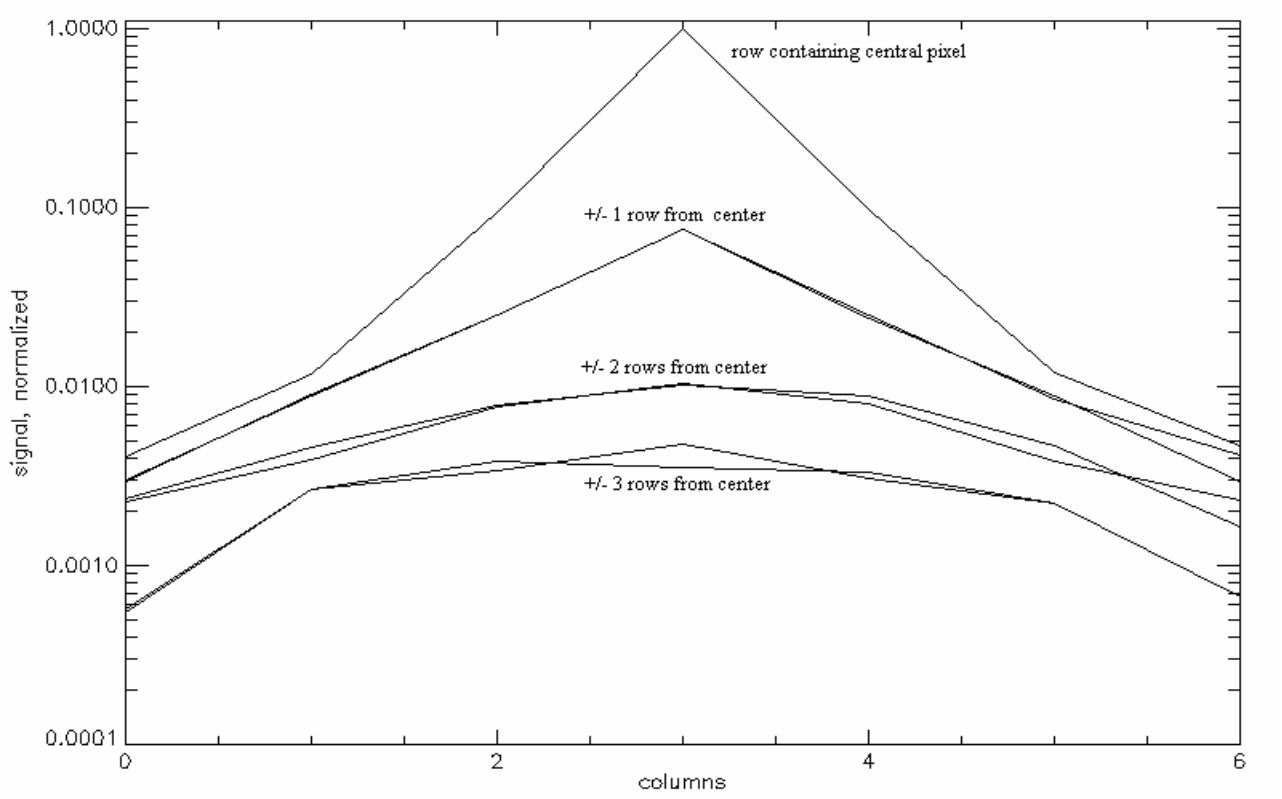

Figure 4a. Line plot through an average proton transient in the detector with substrate

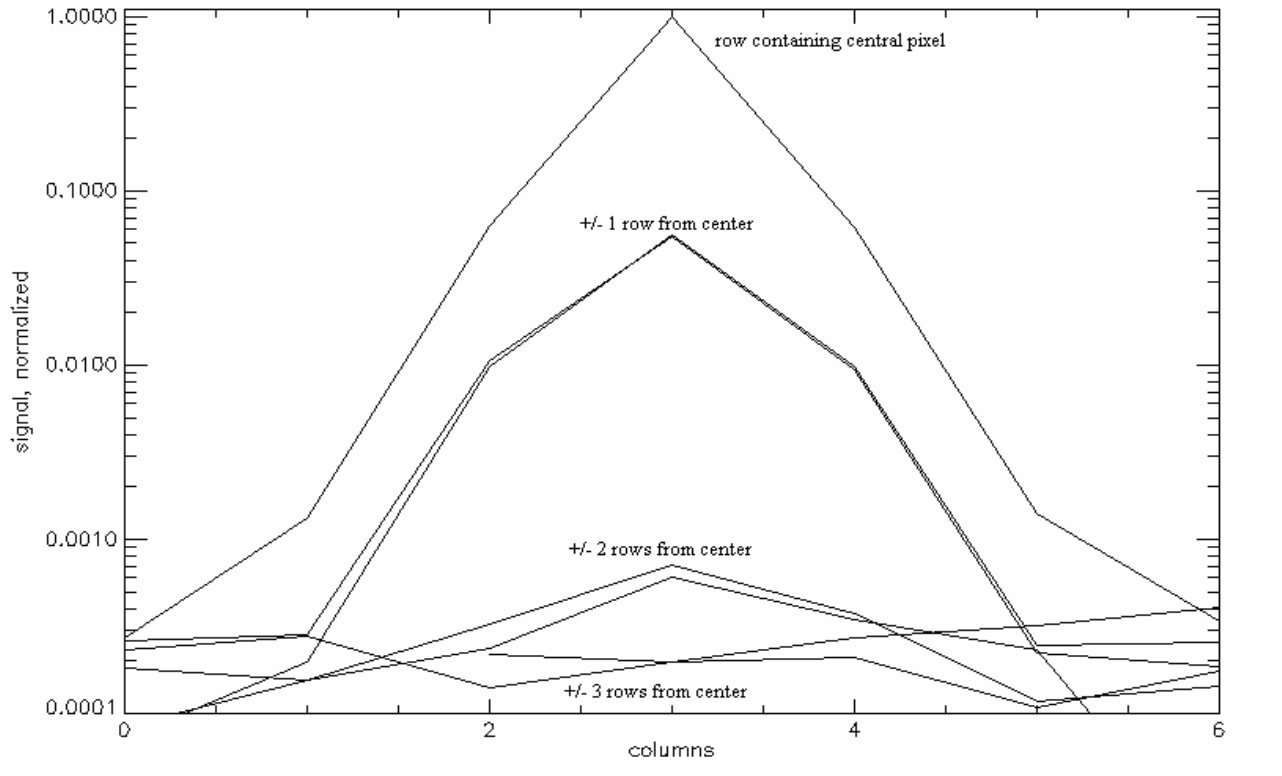

Figure 4b. Line plot through an average proton transient in the detector without substrate

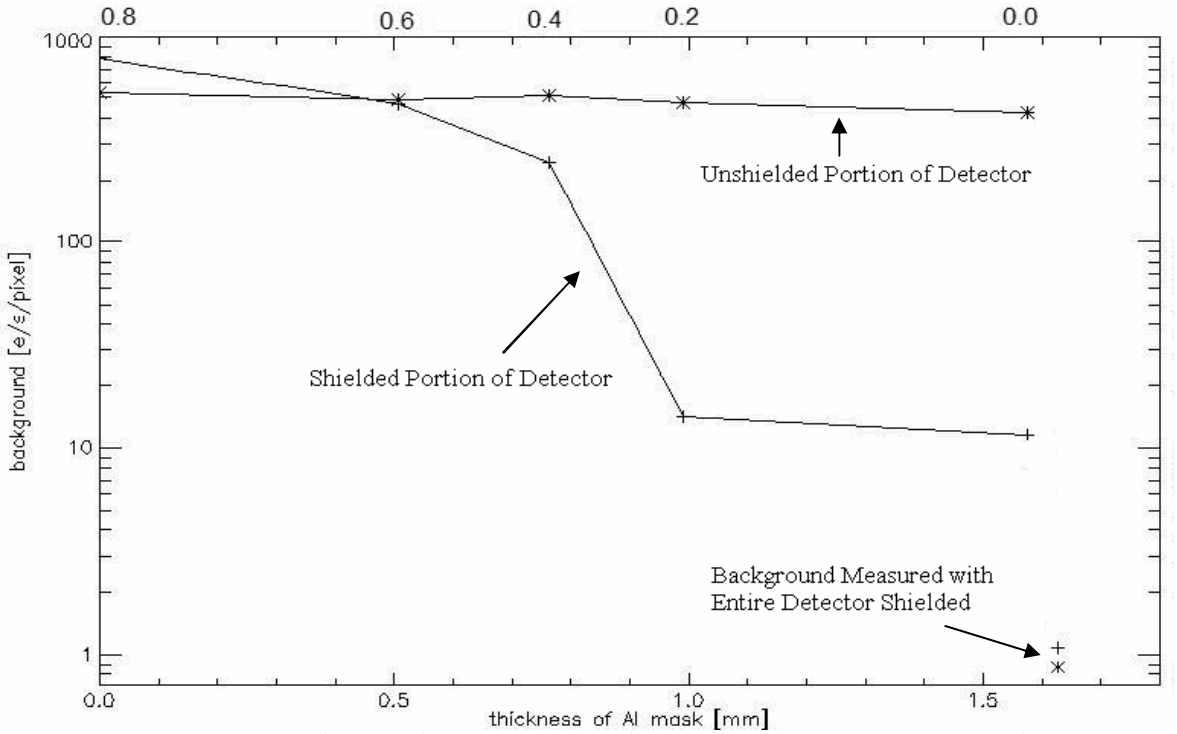

Figure 5. The background changes as a function of proton penetration of the CdZnTe substrate. The lower part of the detector is shielded with varying thicknesses of aluminum shields. The top scale indicates the estimated fraction of the substrate depth penetrated by the beam.

The source of the background has been identified by probing the detector layers with proton beams of varying energy and therefore varying penetration depths. Proton transport through the detector layers was simulated with Monte Carlo Code SRIM. At 15.7 MeV, the protons penetrate only about 80% of the substrate thickness and cannot reach the HgCdTe photodiodes (see Figure 6), as confirmed by the absence of localized transient signatures of individual proton hits, yet images clearly show the presence of increased background signal (first data point in Figure 5).

In the next series of tests, the lower half of the array was shielded with varying thicknesses of aluminum to produce several steps of the penetration depth and amount of energy deposited in the substrate. Figure 5 shows background as a function of shield thickness for the lower part of the array with upper part shown for the reference. While the unshielded part stays relatively constant, the shielded part's background decreases almost linearly with increasing thickness of the shield. It is interesting to notice that the slope of the background changes when the thickness increases and penetration becomes shallower. This may indicate that for shallow penetration, a larger portion of reemitted photons are absorbed in the substrate before they reach the photodiodes. Absorption in the substrate may be a reason why there is only insignificant reduction in background between 1.0 mm and 1.57 mm shield thicknesses.

Another interesting aspect of Figure 5 is that for the 1.57 mm shield thickness, the beam is stopped in the Al shield before it reaches the substrate, but the background under the shield is still significant (at least 10 times larger than expected dark current value). It goes down to the expected dark current level only when the whole detector is shielded by 1.57 mm (shown as the last point in the plot). This implies that some of the background photons can propagate across distances covering at least half of the array (9 mm) from the point of origin.

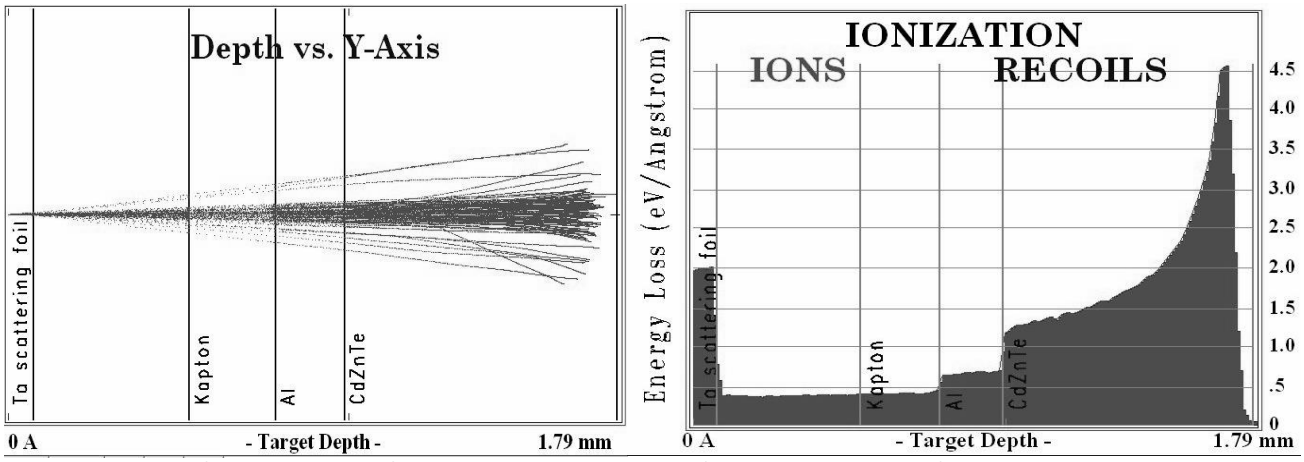

Figure 6. Example of SRIM simulation for 15.7 MeV without addition of Al shield thickness: Left window shows proton beam penetration through the components of the test setup, Al shield and through CdZnTe substrate. The window on the right shows proton energy losses in each of the layers. Notice that the beam stops in the CdZnTe substrate and cannot reach the HgCdTe detector layer.

Additional tests with tuned proton energy of 29.9 MeV were used to test how the background depends on the radiation spectrum. This energy was selected for the reason that it penetrates all detector layers and in this sense is similar to the previously used 63.3 MeV, but its energy deposition rate is approximately twice that of the 63.3 MeV protons. Results confirmed the expectation that background is to first order proportional to the Linear Energy Transfer (LET), and therefore the amount of ionizing dose deposited in the substrate (see Figure 7).

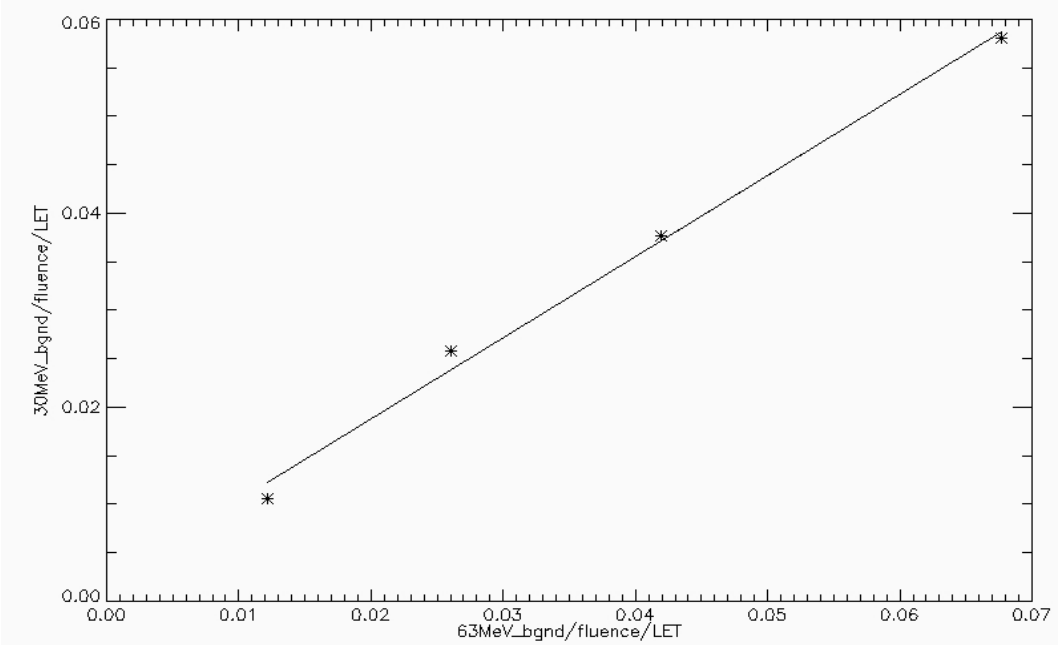

Figure 7. The background at 30MeV normalized to the fluence and LET versus the same for 63 MeV. Slope of the fit line equals 0.88.

The effective radius of the background was further explored by acquiring images with different masks (half plane, small square opening, and horizontal slit) placed in front of the detector. Figure 8 shows the background and fluence profiles using the half plane mask with proton energies of 30 MeV and 15.7 MeV (the square opening and horizontal slit produced equivalent results).

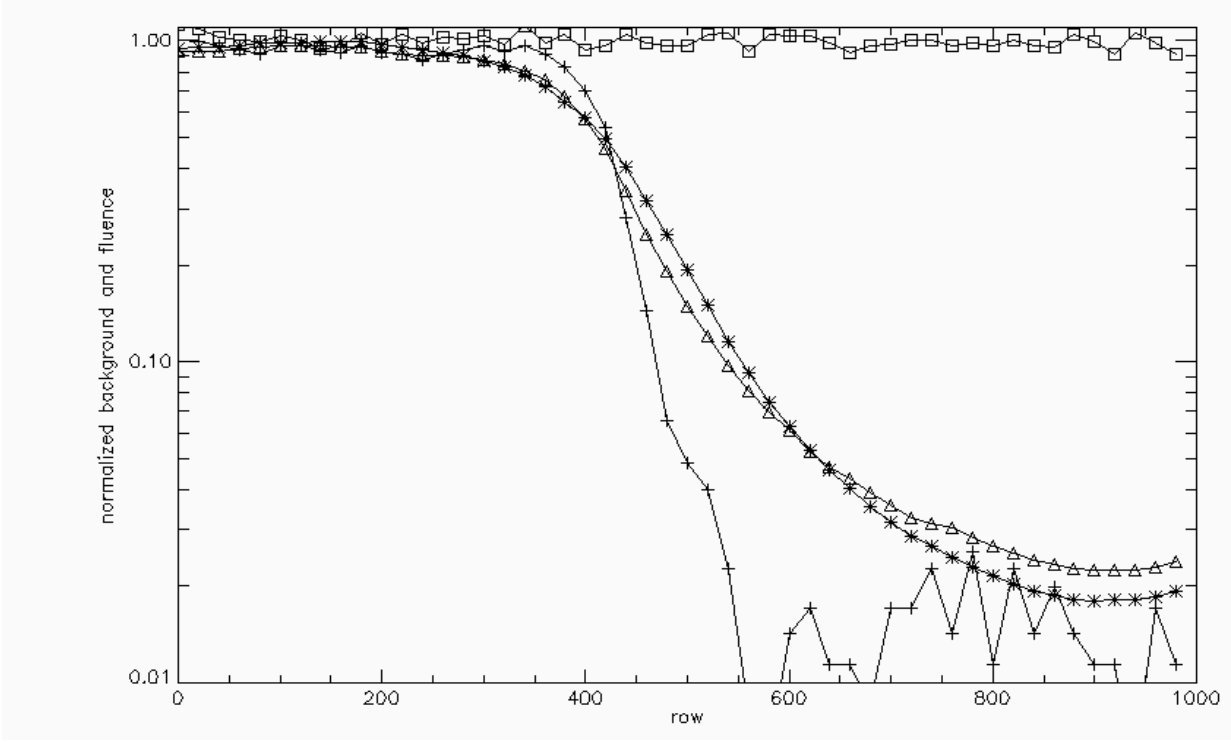

Figure 8. Background and proton fluence profiles for half shielded detector. Starred line and line with triangles show normalized background for 15.7 MeV and 30 MeV respectively, while line with crosses shows normalized fluence. Line with square marks shows fluence profile for unshielded exposure.

As shown in Figure 2, the background distribution across the detector area is highly non-uniform. The fluence profiles for the shielded portion of the detector were therefore normalized to the fluence profile obtained with the entire detector exposed to the beam in order to remove spatial variation of the luminescence effect. Good beam stability was observed throughout testing, and the ratio obtained in normalization was near unity. The two experiments demonstrated that the background induced in the unshielded half of the detector propagates to the other edge of the detector with a magnitude of 2%. The residual level of radiation detected in the shielded part of the detector results from the activation of the detector package and cryostat from previous exposures and does not contain direct proton transients (this follows from the difference in transient magnitude distributions for the shielded and unshielded areas).

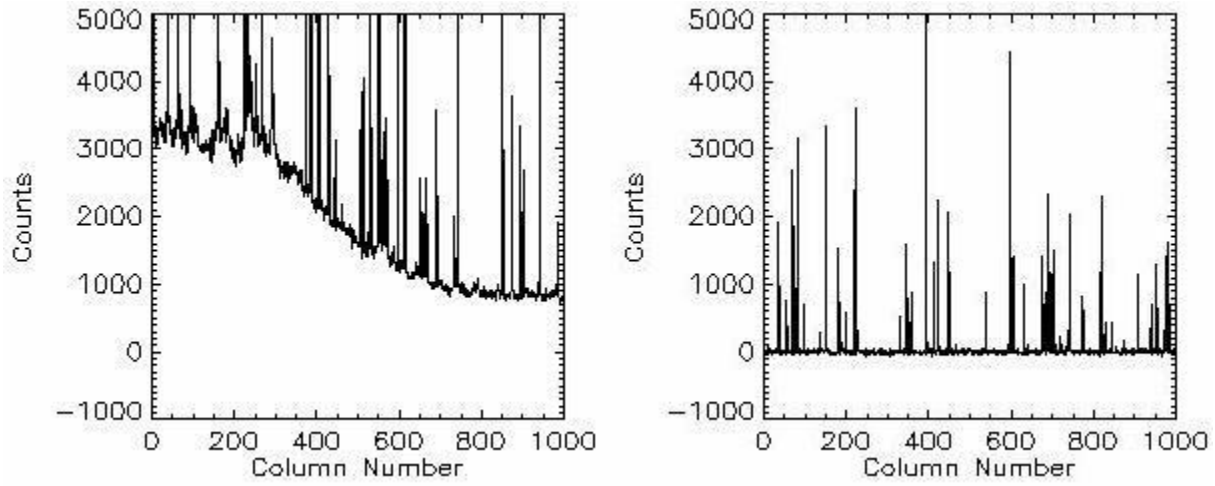

Figure 9. Line plots of FPA67 with substrate (left) and FPA94 without substrate (right) show that removal of the substrate eliminates proton-induced background.

Results of this radiation testing provided conclusive evidence that substrate luminescence is responsible for radiation-induced background. Consequently, WFC3 acquired new detectors with substrate removed and repeated the radiation testing with two of these devices. Figures 4a and 4b compare proton transient images of the new and old detectors, and Figure 9 shows a comparison of line plots for each type of device: there was no evidence of the additional background in the detectors without substrate.

6. DISCUSSION

Table 1. Summary of test results for detectors with and without substrate

	FPA52 (standard substrate)	FPA67 (standard substrate)		FPA94 (no substrate)
Proton Energy [MeV]	63	30	63	63
Direct proton charge [ke]	3	10	5	2
Integrated background per proton [ke]	59	70 to 400	35 to 206	<0.05
Energy left in substrate (Es) [MeV]	3.84	8	3.84	NA
Background normalized to Es [e/eV]	0.015	0.009 to 0.05	0.009 to 0.051	NA

Note: CdZnTe substrate has a thickness of 0.8 mm

Original transient images of FPA52 collected in November 2002 indicated that the interaction of a single 63.3 MeV proton with the detector results in approximately 3000 electrons of charge deposited in the central pixel and 59,000 electrons deposited as an additional background integrated over all pixels. This detector had relatively low overall QE, and at around 800 nm the QE was approximately 10%.

In the second round of testing in May 2004, FPA67 had much better QE and the 800 nm response was close to four times of that in FPA52. This time, the average charge deposited by a proton strike in the central pixel was equal to 6000 electrons, while the integrated background charge was between 35,000 and 206,000 electrons, depending on location. The magnitude of the deposited background and its spatial distribution (see Figure 2) both correlate with the detector quantum efficiency, and they point to the photonic nature of the correlation of proton energy transfer (LET) in the CdZnTe substrate with the amount of charge detected by HgCdTe photodiodes.

Probing the detector layers with varying proton energy has demonstrated that additional background signal is present whenever protons are allowed to interact with the CdZnTe substrate material. It appears to be proportional to LET, and it disappears as soon as the beam falls short of reaching the substrate. Subsequent experiments with substrate-removed detectors have shown that the radiation induced-background has been eliminated.

This constitutes conclusive evidence that ionizing radiation interacts with the CdZnTe substrate and produces a flux of photons which in turn is detected by the HgCdTe photodiodes. The mechanism of converting proton energy into photonic emission in the CdZnTe is not presently fully understood. The results imply that photons emitted from the substrate have wavelengths of approximately 800 nm, which corresponds to the absorption edge of CdZnTe and further implies that some of the photons originating at the top of the 0.8 mm thick substrate will be absorbed while traveling through the remaining substrate thickness toward the detector layer.

A 63.3 MeV proton loses 0.48eV/Angstom in the substrate material, or 3.84 MeV per total substrate thickness. That energy, if completely converted into 800 nm radiation, would result in 2.48×10^6 photons. Assuming 2π field of view and isotropic photon emission, approximately half of that number could reach the detector layer. At the same time, the detector is recording 2.06×10^5 electrons per proton as a maximum response. If we disregard absorption losses in the substrate and assume that the detector quantum efficiency is 100%, we would conclude that the process efficiency for energy conversion from ionization to photon generation is at least 16%. Since the detector's quantum efficiency is lower than 100% and transport through the substrate results in a loss of photons, the conversion efficiency from LET to photons appears to be higher than 16%.

In the third round of testing in December 2004, substrate-removed detectors FPA94 and FPA95 were used. Detector responsivities were good and similar to that of FPA67 in the 0.8 to 1.7 μm range. In addition, removal of the substrate extended the detectors' spectral response down to 350 nm, making them even more capable of detecting any luminescence. Subsequent radiation testing with varying flux and fluence levels yielded negative results: no additional

background was detected, with detection error less than 50 e-/proton, as shown in Table 1. Any residual radiation background, if it still does exist, would have to be approximately three orders of magnitude lower and its impact on the WFC3 instrument performance would be negligible.

7. SUMMARY

Proton induced luminescence in CdZnTe substrates produces a large background signal. Charge deposited in the detector diodes by luminescence exceeds the charge deposited by direct ionization by more than an order of magnitude. The increased background signal is highly non-uniform across the detector area for the sample used in our study, and its spatial distribution is similar to that of the quantum efficiency measured at short (~800 nm) wavelengths. Experimental results indicate that luminescence is proportional to the proton energy loss in the substrate and it appears to correlate with proton LET within the tested range of 15 MeV to 63 MeV. The mechanism of that phenomenon is not understood. We believe that proton interaction with CdZnTe results in the emission of short wavelength photons which in turn propagate and are captured by the HgCdTe photodiodes.

Radiation testing of substrate-removed devices has shown that the luminescence problem is thereby eliminated, with very tight upper limits on any residual diffuse background induced by high energy particle impacts. Scaling these results to the HST orbital environment indicates that, by flying an IR detector with CdZnTe substrate removed, the application induced diffused background can be made negligible for the WFC3 application.

ACKNOWLEDGEMENTS

We would like to acknowledge the support of the Hubble Space Telescope / Wide Field Camera 3 Program, the NASA Electronic Parts and Packaging Program, and the Defense Threat Reduction Agency Radiation Hardened Microelectronics Program. We also appreciate technical support from Greg Delo, Sam Reed, John Yagelowich, Anne Marie Russell, Yiting Wen, and Elizabeth Polidan from GSFC NASA.

REFERENCES

1. Scott D. Johnson, “Radiation effects in WFC3 IR detectors” Proc. SPIE Int. Soc. Opt. Eng. 5167, 243, 2004.
2. Swati Jain, “Photoluminescence Study of Cadmium Zinc Telluride”, MS thesis, West Virginia University, 2001.
3. http://www.rockwellscientific.com/imaging/ROIC_Ref_Table.html
4. http://www.srim.org